2019 NDIA GROUND VEHICLE SYSTEMS ENGINEERING AND TECHNOLOGY SYMPOSIUM
Materials & Advanced Manufacturing (M&AM) TECHNICAL SESSION
AUGUST 13-15, 2019 - NOVI, MICHIGAN

Rigorous Accelerated Approach to Thermomechanical Processing Optimization for New Ballistic Protection Alloys

Thomas Lillo, PhD[1], Henry Chu, PhD[2], Jeffrey Anderson [3], Jason Walleser [3], Victor Burguess [4]

[1]Materials Science and Engineering, Idaho National Laboratory, Idaho Falls, ID
[2]Defense Systems, Idaho National Laboratory, Idaho Falls, ID
[3]SMC Engineering & Product Development, Idaho National Laboratory, Idaho Falls, ID
[4] Ground Vehicle Survivability and Protection, Ground Vehicle Systems Center, U.S. Army Combat Capabilities Development Command, Warren, MI

ABSTRACT

The armor research and development community needs a more cost-effective, science-based approach to accelerate development of new alloys (and alloys never intended for ballistic protection) for armor applications, especially lightweight armor applications. Currently, the development and deployment of new armor alloys is based on an expert-based, trial-and-error process, which is both time-consuming and costly. This work demonstrates a systematic research approach to accelerate optimization of the thermomechanical processing (TMP) pathway, yielding optimal microstructure and maximum ballistic performance. Proof-of-principle is being performed on titanium alloy, Ti-10V-2Fe-3Al, and utilizes the Hydrawedge® unit of the Gleeble 3800 System (a servo-hydraulic thermomechanical testing device) to quickly evaluate mechanical properties and simulate rolling schedules on small samples. Resulting mechanical property and microstructure data are utilized in an artificial intelligence (AI) based response surface methodology (RSM) to identify processing-microstructure-property relationships and develop thermomechanical schedules which are applied to a few larger plates for ballistic testing. This systematic process may reduce the number of TMP schedule permutations by more than 90%. Results to date on Ti-10V-2Fe-3Al and AF9628 will be presented to demonstrate the approach.

.

Citation: T. Lillo, H. Chu, J. Anderson, J. Walleser, V. Burguess, "*Rigorous Accelerated Approach to Thermomechanical Processing Optimization for New Ballistic Protection Alloys*", In *Proceedings of the Ground Vehicle Systems Engineering and Technology Symposium* (GVSETS), NDIA, Novi, MI, Aug. 13-15, 2019.

1. INTRODUCTION

Traditionally, armor materials and systems have been based on strong, hard and relatively dense materials. One of the primary properties in ballistic performance is, unfortunately, density based on the momentum exchange principle. However, high-areal density armor systems compromise vehicle agility, speed and fuel efficiency. Other material properties, such as strength, hardness and ductility, have ill-documented effects on ballistic performance. However, hardness seems to be important. For example, steel-based armor systems tend to utilize high-hardness steel alloys that show greatly improved ballistic efficiency over metal systems with much lower hardness. Also, a recent ARL report showed that hardness in Ti-alloy armor plates, arising from differences in thermomechanical processing, exhibited a significant influence on ballistic performance [1]. Ceramic/metal laminate systems exhibit particularly good performance due to the hard ceramic impact face.

However, it is not known to what extent an optimum mix of these other materials properties will improve ballistic performance in metal-based systems to afford lower areal density vehicular armor systems. (Reduction in armor weight will also enhance the rapid deployment of military assets using existing airborne and marine transports). These material properties are a function of microstructure [2] which is ultimately a result of the thermomechanical processing history, i.e., they are processing path dependent, which can entail a very large number of processing variables, such as casting conditions, rolling or forging temperature and the associated reductions, and final heat treatment(s). As an example, Ti-10V-2Fe-3Al is currently processed for structural applications by rolling at temperatures, (T), above and below the β transus temperature (~800°C) with the amount of reduction (R) at both temperature variables (i.e., T_1, R_1, T_2, and R_2). This rolled material is then subjected to a two-step heat treatment with variable time (t) at each temperature (i.e. T_3, t_1, T_4 and t_2). Thus, the thermomechanical processing schedule for this alloy includes 8 different processing parameters. In the search for the optimum combination of processing parameters, over 65,000 permutations would have to be investigated if only four values for each parameter were used! New statistics-based approaches, such as Design of Experiments (DOE) and machine learning/artificial intelligence (AI) methods, can be used to effectively reduce the number of permutations that need to be studied before the optimum combination can be identified.

The metallic armor research and development community must utilize these advanced statistics-based approaches to accelerate development of new alloys for vehicular armor applications, especially lightweight armor applications. Currently, the development and deployment of new armor alloys is based on “prior experience and build-and-shoot” trial-and-error process, which is both time-consuming and costly, involving fabrication of relatively few bulk alloy samples, characterization of materials properties and, ultimately, ballistic tests. In light of recent advances in rapid computational methods for design of new alloys, rapid methods for determining the optimum thermomechanical processing schedule need to be developed to keep pace with new alloy development and enable deployment of advanced armor systems in a timely manner to mitigate advances in ballistic threats to ground vehicles.

The study reported here focuses on the rapid mapping of thermomechanical processing/property relationships. The approach utilizes testing of small samples to minimize the costs associated with custom alloy production. Ultimately, the goal of this work is to be able to predict thermomechanical processing parameters that yield targeted mechanical properties, which can then be used to systematically determine mechanical property/ ballistic property relationships (and subsequently be able to relate thermomechanical processing to ballistic performance), and ultimately identify the optimum thermomechanical processing schedule for the best ballistic performance of emerging alloys designed to reduce overall vehicle weight with equivalent or increase ballistic protection.

2. Experimental Approach

The goal of the work is to investigate thermomechanical processing (TMP) of alloys on a lab scale to identify processing parameters suitable for full-scale processing. The first step is the breakdown of the cast structure and is typically accomplished by rolling or forging of a large casting consisting of a large-grain cast structure potentially with considerable macro-segregation of the alloying elements. The challenge is to roll or forge the cast billet without creating catastrophic defects such as macro-cracks and delaminations. Thus, identification of suitable rolling or forging parameters that result in a defect-free, homogeneous plate is of paramount importance. Doing this rapidly and economically is the first focus of this study which is aimed at identifying the TMP envelop for producing sound plate. The second focus of this study is to map this TMP space to final mechanical properties to allow the systematic study of the correlation between mechanical properties and ballistic performance.

Various aspects of the approach will be demonstrated on two widely different alloys – Ti-10V-2Fe-3Al and AF9628 steel. Compositions, in weight percent, are given in Table 1.

Table 1: Nominal Alloy Compositions, wt%

	AF9628	Ti-10V-2Fe-3Al
Carbon	0.28	≤0.05
Chromium	2.5	
Molybdenum	1	
Vandium	0.2	10
Manganese	≤1	
Nickel	≤3	
Silicon	≤1.25	
Copper	≤0.15	
Phosphorous	0.015 max	
Sulfur	0.02 max	
Calcium	0.02 max	
Nitrogen	0.15 max	≤0.05
Oxygen		≤0.13
Hydrogen		≤0.015
Aluminum	0.025 max	3
Iron	Balance	2
Titanium		Balance

2.1. Thermomechanical Processing

To map the TMP space, small samples of the alloys are tested in the Gleeble 3800, a universal, servo-hydraulic testing machine. Initially, the flow stress behavior at various temperatures and strain rates relevant to TMP is determined by compression tests of samples with dimensions of 14.25 mm in diameter by 18.1 mm tall for alloy, Ti-10V-2Fe-3Al, and 10 mm in diameter by 12 mm tall for the steel alloy AF9628. Larger samples were used for the Ti alloy due to the larger starting grain size in this cast alloy to ensure the number of grains is sufficient to adequately represent the true flow stress of the alloy. The test matrix for each alloy is shown in Tables 2 & 3. Tests were carried out to a true strain of -0.65 for Ti-10V-2Fe-3Al samples and a true strain of -0.5 for the AF9628 samples, corresponding to reductions in thickness of 48% and 40%, respectively. An example of the AF9628 samples before and after compression are shown in Fig. 1.

Examples of the compression data for both alloys are shown in Fig. 2. From the compression data, flow stress as a function of strain rate at a given value of true strain are plotted to reveal the strain

Table 2: Compression Test matrix for Ti-10V-2Fe-3Al

Temperature, °C	True Strain Rate, s^{-1}				
	0.1	0.3	1	3	10
700	x	x	x	x	x
750	x	x	x	x	x
800	x	x	x	x	x
850	x	x	x	x	x
900	x	x	x	x	x

Table 3. Compression Test matrix for AF9628

Temperature, °C	True Strain Rate, s^{-1}				
	0.1	1	5	10	50
900	x	x	x	x	x
1000	x	x	x	x	x
1100	x	x	x	x	x
1175	x	x	x	x	x

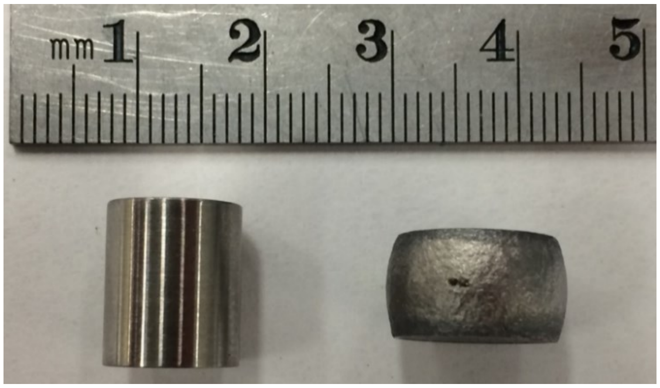

Figure 1: Example of the AF9628 sample before and after compression testing.

rate sensitivity, m, the slope of the flow stress curves in Fig. 3. For both alloys the strain rate sensitivity, m, is a function of strain rate as indicated by the non-linear curves at each temperature. The curves in Fig. 3a for AF9628 are fairly uniform and similar while the curves in Fig. 3b, vary significantly over the temperature range suggesting different mechanisms are responsible for microstructural change, e.g., cracking, shear banding, dynamic recrystallization, etc. Theory on the development of deformation processing diagram from the strain rate sensitivity is described in detail elsewhere [3,4] but ultimately depends on mapping the efficiency, η, of power dissipation due to microstructural change which is given in [4]:

$$\eta = \frac{2m}{(m+1)} \tag{1}$$

Furthermore, Prasad et al. [3], shows that regions of microstructural instability can be mapped on to this deformation processing diagram using:

$$\xi(\dot{\varepsilon}) = \left\{ \frac{\partial ln\left(\frac{m}{(m+1)}\right)}{\partial \dot{\varepsilon}} \right\} + m < 0 \tag{2}$$

where $\dot{\varepsilon}$ is the true strain rate. Thermomechanical processing schedules for forming the alloy should be designed to avoid these regions.

2.2. Deformation Processing of AF9628

No previous attempts had been made to roll this alloy as its targeted application required forging. Therefore, a deformation processing map was developed for applications amenable to rolling. The deformation processing diagram, based on the Gleeble-based compression tests for AF9628, is shown in Fig. 4. Regions of microstructural instability, i.e., the red boxes, are indicated only for relatively high and low temperatures at either relatively high or low strain rates. Therefore, the TMP parameters associated with the central region of this map can be used to process this alloy - from approximately 975°C-1125°C and strain rates ranging from ~1 s^{-1} to ~10 s^{-1}. Most conventional rolling schedules and rolling equipment tend to use reductions that use strain rates between 1-10 s^{-1} and, therefore, this alloy should roll without issues

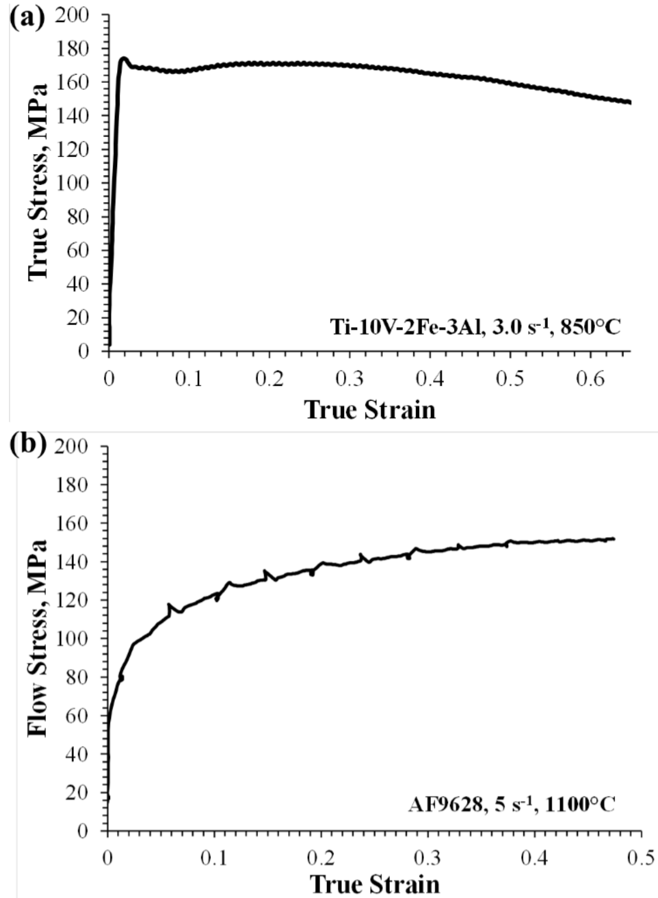

Figure 2: Examples of the compression data for (a) Ti-10V-2Fe-3Al and (b) AF9628. Fast data collection rates are responsible for the irregularities in the plots.

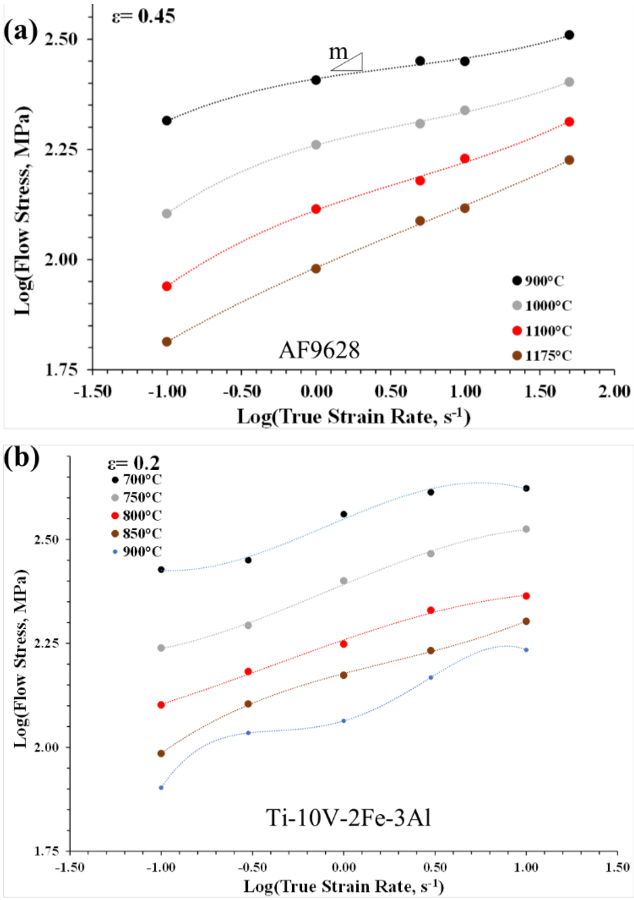

Figure 3: Plots of the sensitivity of the flow stress to strain rate with a 3rd order polynomial curve fit for each temperature. The strain rate sensitivity, m, at a given strain rate is the slope of the line.

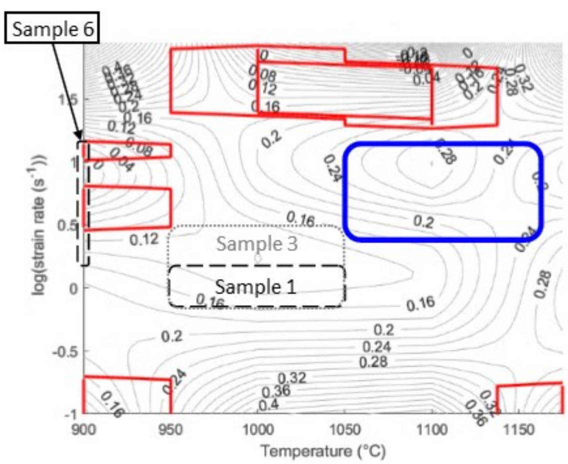

Figure 4: Deformation processing map (ε=0.45) with regions of microstructural instability, in red, for AF9628, actual rolling conditions, blue, and processing envelops for Samples 1, 3 and 6, dotted black and grey.

of cracking, localized shearing or adiabatic shear banding. Rolling simulations using various deformation schedules were carried out in the Gleeble 3800 which also can simulate the plane strain conditions of a rolling mill. An example of a sample being subjected to simulated rolling in the Gleeble is shown in Fig. 5. Rolling simulation samples of AF9628 were 20 mm wide by 10 mm thick and 60 mm long. The simulated rolling schedule of selected samples are given in Table 4 with micrographs from the polished and etched cross section of each sample shown in Fig. 6. Sample 1 in Table 3 simulates a 50% reduction in thickness in nine passes, starting at 1050°C and finishing the last pass at 950°C. The strain rate for each pass was around 1 $s^{-1}$and fell within the processing envelop shown in Fig. 4, labeled as "Sample 1". Sample 3 simulated a 74% reduction in thickness in 15 passes, starting at 1050°C and finishing the last pass at 950°C. An intermediate reheat was inserted into this schedule to more accurately simulate an actual rolling schedule. The processing envelop of Sample 3 is also shown in Fig. 4 and labeled "Sample 3". Finally, Sample 6 was designed to intentionally produce sample failure. Simulated rolling of this sample was carried out at 900°C with relatively high strain rates (~10-15 s^{-1}) to achieve a 50% reduction in thickness. These conditions contain the predicted regions of instability at the left of the deformation processing diagram in Fig. 4. None of the samples catastrophically failed, however, Samples 1 and 6,

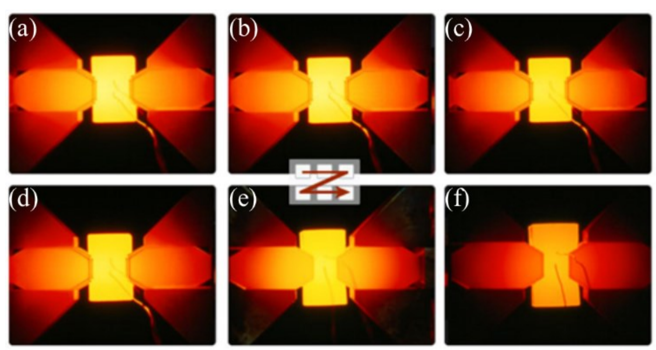

Figure 5: A sample in the Gleeble 3800 being subjected to a series of simulated passes (a)-(f) through a rolling mill.

Table 4: Processing schedules for simulated rolling study

Sample ID	Rolling pass #	Temperature, °C	True Strain Rate, s^{-1}	Cumulative true strain	Cumulative reduction, %
1	1	**1050**	0.80	0.04	3.7
	2		1.18	0.11	10.8
	3		1.28	0.20	18.0
	4		1.31	0.28	24.4
	5		1.66	0.40	32.8
	6		1.49	0.48	38.3
	7		1.45	0.56	42.8
	8		1.48	0.63	46.8
	9	**950**	1.35	0.69	49.7
3	1	1050	0.80	0.04	3.70
	2		1.18	0.11	10.83
	3		1.28	0.20	18.05
	4		1.31	0.28	24.44
	5		1.66	0.40	32.83
	6		1.49	0.48	38.34
	7		1.45	0.56	42.78
	8		1.48	0.63	46.78
	9	950	1.35	0.69	49.71
	Anneal 15 minutes at 1050°C (simulates re-heat)				
	10	1050	2.1	0.82	55.7
	11		1.9	0.91	59.7
	12		2.0	1.00	63.4
	13		2.1	1.10	66.6
	14		2.7	1.24	70.9
	15	950	2.8	1.36	74.4
6	1	900	15.00	0.36	30.00
	2		10.00	0.52	40.50
	3		1.65	0.62	46.45
	4	900	1.74	0.70	50.20

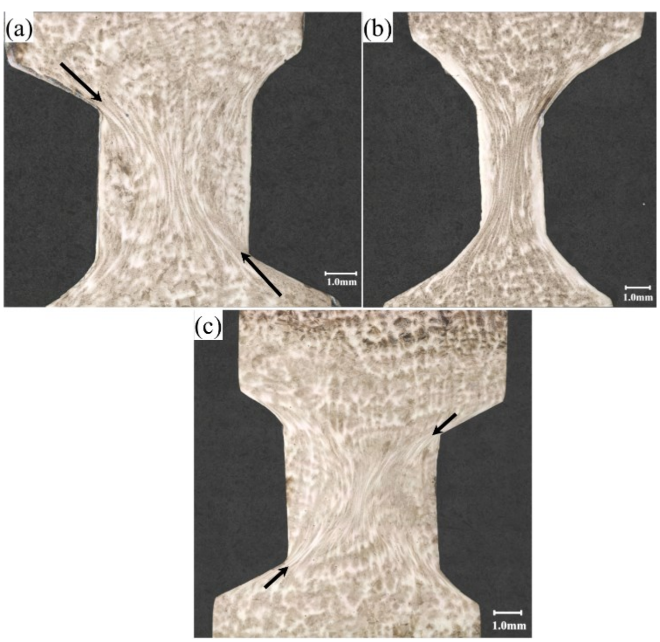

Figure 6. Etched cross sections of samples from the rolling simulation, (a) Sample 1, (b) Sample 3 and (c) Sample 6. Black arrows denote shear band failure in (a) and (c).

appear to exhibit localized shear, possibly adiabatic shear banding at the arrows in Figs. 6a and 6c. This is expected for Sample 6 but not for Sample 1, based on the position of the processing envelop in Fig. 4. However, the deformation processing map in Fig. 4 was generated for ε=0.45, while Sample 1 was processed to a final strain of 0.69 suggesting that the deformation processing map at ε=0.69 has regions of instability that fall within the processing envelop of Sample 1. In light of this observation, a conservative envelop for full-scale rolling was defined at higher temperatures, indicated by the blue box on Fig. 4. Four-inch thick, 400 lbs, as-cast billets of AF9628 were commercially rolled to reductions in thickness of 50%, 75%, 88% and 94% using conditions within this more conservative processing envelop. All billets were rolled quickly and successfully without any evidence of cracking, even edge cracks, or localized shear, Fig. 7. This successfully demonstrated the ability of the approach to identify suitable rolling parameters, reduce the tendency for rolling defects and, thereby, maximize production yields. No further optimization of the TMP parameters for mechanical properties is currently planned for this alloy.

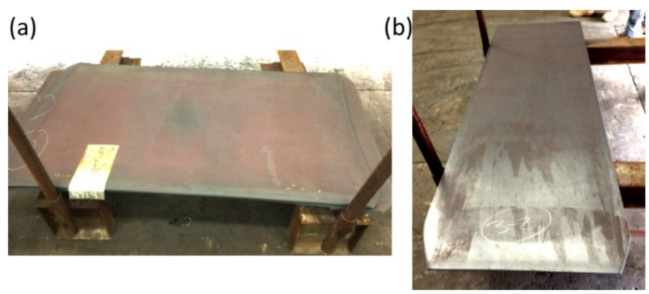

Figure 7: Rolled AF9628 plate, (a) 0.5" and (b) 0.25" thick.

2.3. Deformation processing of Ti-10V-2Fe-3Al

Work is underway to develop TMP/mechanical property relationships for Ti-10V-2Fe-3Al, including optimization using AI methods, with the eventual goal of establishing TMP/ballistic performance relationship and optimization. The approach for developing the deformation processing diagram for AF9628 was also used for this Ti-based alloy. Figure 3b shows the log(strain rate) vs. log(flow stress) curves exhibit considerable variation with temperature. (Beyond ε=-0.2, some combinations of strain rate and temperature caused the samples to catastrophically fail and yield inaccurate flow stress values. Thus, development of the deformation map was carried out at ε=0.2.) This is likely due to the allotropic transformation at ~800°C. Below 800°C, the microstructure is a mixture of α and β Ti while above 800°C only the β phase is stable. The flow behavior in Fig. 3b results in a deformation processing diagram as shown in Fig. 8. This is considerably different from the deformation processing diagram given by Balasubrahmanyam, et al. [4]. However, that diagram was developed using a wrought Ti-10V-2Fe-3Al material as opposed to the cast material used in this study, Fig. 9, and, therefore, has a considerably different microstructure, which can significantly affect the appearance of the deformation processing diagram [5].

From this deformation processing diagram, rolling schedules are being developed and simulated on the Gleeble. To date, simulated rolling schedules, shown in Table 5, have been carried out as part to the thermomechanical optimization study. The schedules included reductions both above and below the β transus of this alloy (~800°C), which is standard mill practice for most titanium alloys [6]. The two schedules only differ in the rolling temperature below the β transus and can be generally described by the green and blue boxes in Fig. 8. Both simulated rolling schedules resulted in successful deformation without any visible defects, such as fractures, Fig. 10a, b.

After rolling, the material is subjected to a two-step heat treatment to obtain desired microstructure and mechanical properties. The shape of the Gleeble rolling simulation samples allows mini-flat tensile bars, 1.5 mm thick, to be sliced off using electro-discharge machining (EDM), Fig. 10c, typically producing 8-9 tensile samples for

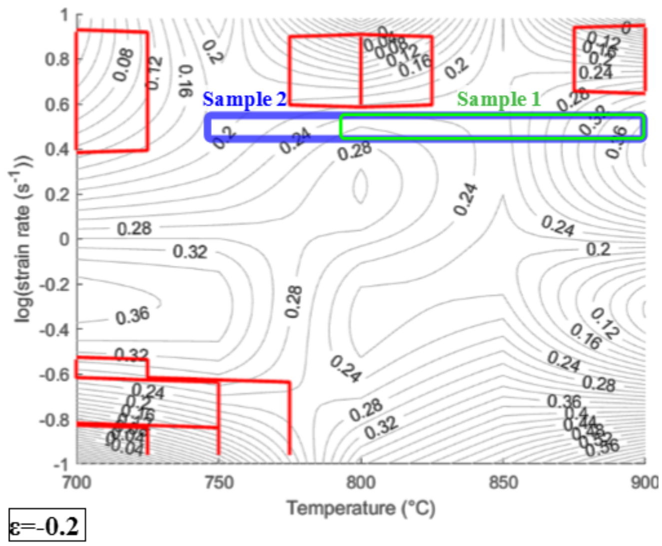

Figure 8. Deformation processing diagram for cast Ti-10V-2Fe-3Al.

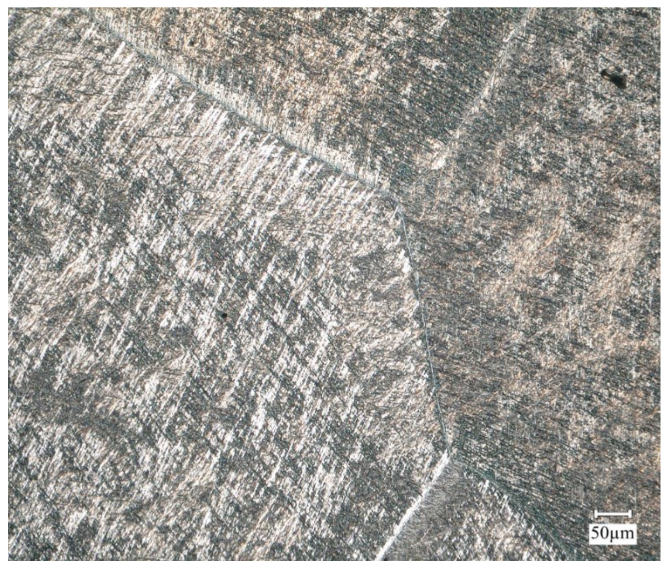

Figure 9. As-cast microstructure of Ti-10V-2Fe-3Al consisting of α-Ti platelets on the grain boundaries and grain interiors.

subsequent heat treated and tensile testing. The goal here is to provide relative mechanical properties as a function of rolling schedule and heat treatment, as these tensile specimens do not conform to ASTM standards. However, tensile specimens generally failed within the reduced section of these flat tensile bars, Fig. 11, confirming the measured tensile

Table 5. Simulated Rolling Schedules Applied to Cast Ti-10V-2Fe-3Al

Sample ID	Rolling pass #	Temperature, °C	True Strain Rate, s^{-1}	Cumulative true strain	Cumulative reduction, %
Sample 1	1	900	3	0.16	0.15
	2	900	3	0.36	0.30
	3	790	3	0.52	0.41
	4	790	3	0.71	0.51
	5	900	3	1.07	0.66
	6	790	3	1.20	0.70
Sample 2	1	900	3	0.16	0.15
	2	900	3	0.36	0.30
	3	750	3	0.52	0.41
	4	750	3	0.71	0.51
	5	900	3	1.07	0.66
	6	750	3	1.20	0.70

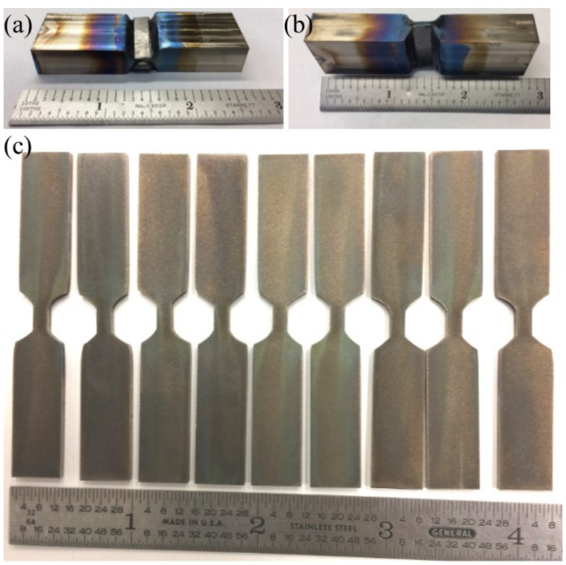

Figure 10: (a) and (b) Simulated Gleeble rolling samples and (c) flat tensile bars produced by EDM.

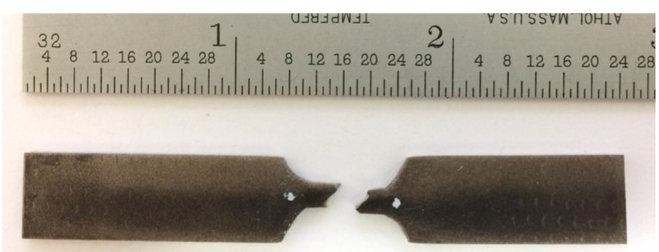

Figure 11. Specimen failure during tensile testing occurred in the reduced section of the mini-flat tensile specimens.

strength was a valid representation of the material. Mechanical property data is used in the AI approach discussed below.

2.4. Artificial intelligence (AI) based response surface methodology (RSM) for processing/property relationships

The experimental work previously discussed is designed to apply potential thermomechanical processing schedules on small samples which, when heat treated, will yield mechanical and microstructural properties and data that can be used to develop processing/property relationships using an AI approach. The use of AI permits process-property mapping without prior assumptions of functional form or linearity.

Support vector regression (SVR), a category of support vector machine (SVM), with radial basis functions was selected to perform the process-property mapping. This technique has the advantage of creating a relatively smooth and optimizable surface that is amenable to a wide range of optimization strategies and has a unique solution [7]. The SVR was implemented using the python scikit-learn library.

There are three meta-parameters that are required as input to the SVR. They are denoted as γ, C, and ε, which correspond to the kernel coefficient, error term penalty parameter, and the error tolerance for which no penalty is assigned. These parameters were selected for models of ultimate stress, strain at fracture and stress-strain area (relating to the energy dissipated during deformation) using a grid-search for each model. The grid search evaluated a range of candidate meta-parameter values by conducting trial training attempts and evaluating performance by calculating a cross validated R-squared value from data that was left out of the training set. The meta-parameters that produced models with the best predictive ability were then used to train the models with the full data set.

The resulting SVR model was then used to find

Table 6: Screening study tensile test results.

Sample ID	Temp. 1, °C	Duration 1, hrs	Temp. 2, °C	Duration 2, hrs	Max Strain, %	Max Stress, MPa	Stress-strain Area, MPa
Ti-700-580	700	4	580	8	17.2	893.3	120.2
Ti-700-500	700	4	500	8	18.0	991.5	125.6
Ti-700-400	700	4	400	8	13.9	1151.9	108.7
Ti-700-350	700	4	350	8	13.7	1089.4	100.1
Ti-650-580	650	4	580	8	17.0	989.4	120.7
Ti-650-500	650	4	500	8	22.1	1033.1	182.7
Ti-650-400	650	4	400	8	20.9	1070.2	170.4
Ti-650-350	650	4	350	8	18.4	1033.4	144.9

the global maxima in each model using the differential evolution optimization algorithm [8]. The SVR model decays to some central value for the data set in areas not populated with experimental data. This prevents excessive extrapolation outside of the bounds of the known data.

Sample plans for generating input data for model training were initiated using two methods. First, a screening study was performed using a traditional orthogonal experiment matrix. Since grid based methods, such as full factorial designs, would require too many samples to be practical when the number of processing variables becomes large, a Latin Hypercube design was also prepared with optimal spacing. The reason for choosing the Latin Hypercube was that it can be implemented in a highly efficient way that helps minimize the effects of the curse of dimensionality, and it is non-collapsing if one or more input variables are found to be unimportant. In contrast to an m^k factorial design, where m is the number of levels and k is the number of factors and the number of samples is $n = m^k$, a Latin Hypercube design only requires around p = 10-20 levels per factor such that $n = pk$. This results in a large reduction in the number of required samples, especially when k becomes large. In this study, k is four (two temperatures and two durations) and with m=4, m^k is 256 while pk is only 40-80. The "curse of dimensionality" becomes apparent when the number of parameters is increased to k=8 which gives $n = m^k = 65536$ and $n=pk$ is 80-160 samples required. This clearly illustrates the benefits of a Latin Hypercube design when the number of factors is more than two or three. A previous Ti-10V-2Fe-3Al TMP study using a similar approach was published by Quan et al. [9] to map hot flow behavior of the material.

The data from the screening study are given in Table 6. Since the durations are held constant, this study has two inputs and one output per model. Uniaxial tensile tests were conducted and maximum stress, strain, and stress-strain curve area were derived from the results. These data were used to fit a separate SVR model for each evaluation metric as shown in Fig. 12. Since the data set was relatively small, the cross-validation technique was skipped for the screening study.

The SVR model fit the data well and appears to effectively combine information about the magnitudes, slope, and curvature information provided by the data to make interpolated predictions. It was also noted in practice that the effective radius of influence of a data point or points was directly affected by the γ parameter. In the model fits shown here, the influence of the data points decays rapidly enough to prevent any significant extrapolation beyond the data set.

The computed maxima for each model are given in Table 7 along with the temperatures at which they occurred. Later work will include SVR mapping of material properties to ballistic performance to determine the optimal balance. For now, it is unclear which variables should be maximized, although it is expected that the area under the stress-strain curve may dominate ballistic performance. However, the strain rate of ballistic events is considerably different compared to those in the tensile tests.

Work has begun on the Latin Hypercube tensile test matrix to more fully refine the predictive qualities of the models. Also, to alleviate concerns related to the reproducibility of the tensile data, three specimens have been subjected to the same

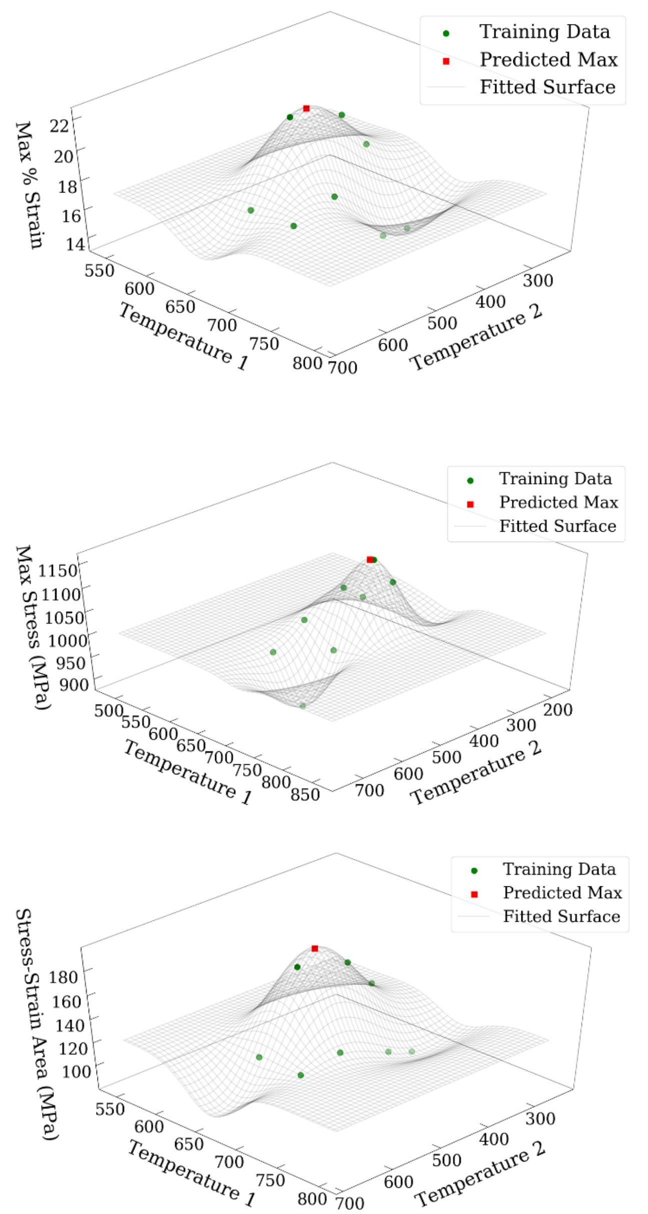

Figure 12: SVR response surface model fits for strain at failure, maximum stress, and area under the stress-strain curve. The units of temperature are °C.

Table 7: SVR RSM optimization results from the screening study for a duration of 4 and 8 hrs, respectively at each temperature.

Evaluation Metric	Temp. 1 °C	Temp. 2 °C	Max Value
Strain, %	647.3	464.6	22.2
Stress, MPa	697.2	406.5	1153.6
Stress-Strain Area, MPa	648.0	462.7	191.4

heat treatment schedule and tensile tested. The results for three different heat treatment conditions are shown in Table 8. For each set of conditions the tensile strength was found to be within ±5% of the average. Also, the ductility was within ±5% of the average for two of the conditions exhibiting double-digit ductility and within ±10% of the average for the condition exhibiting single-digit ductility values. It was, therefore, concluded that the use of the mini-flat tensile bars provides reproducible tensile data for use in the AI analysis and, going forward, multiple samples for each condition are not required.

Table 8. Preliminary tensile properties of three experiments selected from the 4-dimensional Latin Hypercube test matrix.

Sample ID	Temp. 1, °C	Duration 1, hrs	Temp. 2, °C	Duration 2, hrs	Max. Strain %	Max. Stress, MPa	Stress-strain Area, MPa
Ti-674C-626C-1	674	7.1	626	20.6	16.7	817.0	104.6
Ti-674C-626C-2	674	7.1	626	20.6	17.7	870.5	116.6
Ti-674C-626C-3	674	7.1	626	20.6	17.9	853.5	113.4
Ti-722C-493C-4	722	12	493	4.7	12.4	1068.0	90.4
Ti-722C-493C-5	722	12	493	4.7	13.7	1088.3	102.2
Ti-722C-493C-6	722	12	493	4.7	13.2	1082.4	90.1
Ti-751C-372C-7	751	9.3	372	23.3	7.1	926.8	31.0
Ti-751C-372C-8	751	9.3	372	23.3	5.7	866.2	24.5
Ti-751C-372C-9	751	9.3	372	23.3	6.2	930.4	28.6

3. Comments and Future Work

The approach described in this work has been demonstrated to yield suitable TMP parameters to successfully roll alloys where there is little prior processing knowledge. Future work will concentrate on completing the Latin Hypercube-based test matrix to confirm the preliminary results shown here. The AI models will be used to predict TMP/mechanical property relationships and will be the basis for producing full-sized plates with various combinations of mechanical properties which will be used in subsequent ballistic tests to understand the collaborative links between TMP, mechanical properties and ballistic performance and, ultimately, to be able to optimize TMP parameters for optimum ballistic performance, and, thus, minimize areal density for equivalent protection.

4. Acknowledgements

The authors acknowledge the diligent work of Mr. Denis Clark and Joel Simpson for their efforts on the Gleeble work and Mr. Arnold Erickson for heat treating and microstructural characterization.

The Ti-10V-2Fe-3Al work was internally funded through INL's Laboratory-directed Research and Development program under DOE Idaho Operations Office Contract, DE- AC07-05ID14517. Additionally, funding from US Army TARDEC under a work for others agreement, WFO Project #18707 is gracious acknowledged for the work on AF9628.

5. REFERENCES

[1]J. Le, "V_{50} Evaluation of Titanium Alloys Ti-6Al-4V and Ti-10V-2Fe-3Al", US Army Research Laboratory, ARL-CR-0795, March 2016.

[2] Terlinde, G.T., T.W. Duerig, J.C. Williams, The Effect of Heat Treatment on Microstructure and Tensile Properties of Ti-10V-2Fe-3Al, Office of Naval Research, Technical Report, JWTR-8, April 1980

[3]Y. Prasad, T. Seshacharyulu, "Modeling of hot deformation for microstructural control", Int. Mater. Rev., vol 43, pages 243-258, 1998.

[4]V. Balasubrahmanyam, Y. Prasad, "Hot deformation mechanisms in metastable beta titanium alloy Ti-10V-2Fe-3Al", Mater. Sci Tech., vol 17, pages 1222-1228, 2001.

[5]Y. Prasad, "Processing Maps: A Status Report", J. Materials Engg. And Perform., vol. 16, issue 6, pages 638-645, 2003.

[6]G. Lutjering and J.C. Williams, Titanium, Springer-Verlag, New York,

[7] S. Keerthi and C. Lin, "Asymptotic Behaviors of Support Vector Machines with Gaussian Kernel," Neural Computation*,* pp. 1667-1689, 2003

[8] R. Storn and K. Price, "Differential Evolution -- A Simple and Efficient Heuristic for Global Optimization over Continuous Spaces," Journal of Global Optimization*,* pp. 341-359, 1997

[9] G. Quan, Z. Zhang, L. Zhang, and Q. Liu, "Numerical Descriptions of Hot Flow Behaviors across β Transus for as-Forged Ti–10V–2Fe–3Al Alloy by LHS-SVR and GA-SVR and Improvement in Forming Simulation Accuracy," Applied Sciences, vol 6, 2016